CONDENSED MATTER PHYSICS

Rapid isotopic exchange in nanoparticles

Papri Chakraborty[1], Abhijit Nag[1], Ganapati Natarajan[1], Nayanika Bandyopadhyay[1], Ganesan Paramasivam[1], Manoj Kumar Panwar[1], Jaydeb Chakrabarti[2], Thalappil Pradeep[1]*

Rapid solution-state exchange dynamics in nanoscale pieces of matter is revealed, taking isotopically pure atomically precise clusters as examples. As two isotopically pure silver clusters made of ^{107}Ag and ^{109}Ag are mixed, an isotopically mixed cluster of the same entity results, similar to the formation of HDO, from H_2O and D_2O. This spontaneous process is driven by the entropy of mixing and involves events at multiple time scales.

INTRODUCTION

Since the discovery of deuterium (D) (*1*) and the isolation of D_2O (*2*), isotopic exchange in molecules has served as a characteristic signature of their dynamic chemical bonds (*3*). The rate of isotopic exchange in water ($H_2O + D_2O = 2HDO$) is fast with an equilibrium constant of 3.75 ± 0.07 at room temperature (*4*), and it occurs at measurable speeds down to cryogenic temperatures (*5*). H/D exchange in proteins has been an important tool to understand their surface structure (*6*). Moreover, isotopic exchange in systems like H_2/D_2 has high activation barrier and occurs at very high temperatures (~1000 K) or over heated catalytic metal surfaces (*7*). The existence of nanomaterials of noble metals with precise composition (*8*, *9*) allows the feasibility of their isotopic exchange to be tested. Using high-resolution electrospray ionization mass spectrometry (ESI MS), we show that atomically precise monolayer-protected nanoclusters, made of isotopically pure silver (^{107}Ag and ^{109}Ag), despite their well-defined structures and ligand protection, undergo rapid exchange of the isotopes of the metal atoms. The exchange approaches a dynamic equilibrium within a minute in solution at room temperature. Using two archetypal examples of Ag nanoparticles of precise composition, $[Ag_{25}(SR)_{18}]^-$ (*10*) and $[Ag_{29}(S_2R)_{12}(TPP)_4]^{3-}$ (*11*), where SR, S_2R, and TPP are protecting ligands, we demonstrate that the rapid isotopic exchange reflects their solution-state dynamics. In addition, we show the ability to control the exchange dynamics by controlling the temperature. Time-resolved measurements further reveal that the mechanism of exchange involves several processes that occur at different time scales. The spontaneity in such reactions is mainly driven by the mixing entropy contribution to the free energy. Such an exchange mechanism, reminiscent of isotopic exchange between H_2O and D_2O, presents intriguing insights into the nature of nanoscale matter.

RESULTS

To study isotopic exchange, we chose $[Ag_{25}(SR)_{18}]^-$ clusters (*10*) initially. Two identical but isotopically different clusters, $[^{107}Ag_{25}(DMBT)_{18}]^-$ and $[^{109}Ag_{25}(DMBT)_{18}]^-$ (DMBT = 2,4-dimethyl benzene thiol), were prepared starting from isotopically pure metals and extensively characterized to ensure their chemical purity and isotopic identity. The isotopic clusters showed identical optical absorption spectra (fig. S1A). ESI MS of $[^{107}Ag_{25}(DMBT)_{18}]^-$ and $[^{109}Ag_{25}(DMBT)_{18}]^-$ are presented in Fig. 1A, a and b, respectively. The peak maxima of the spectra are separated by *m*/*z* (mass/charge ratio) 50 because of the interchange of 25 atoms of ^{107}Ag with ^{109}Ag. The mass spectral distributions of the isotopic clusters are narrower than those of a sample with natural Ag (fig. S1B). The isotope patterns (fig. S1, C and D) are purely due to the isotopes of S, C, and H in the ligands, and therefore, they are similar to those of the $[Au_{25}(PET)_{18}]^-$ cluster (*12*, *13*) [PET (phenyl ethane thiol) has the same atomic composition ($C_8H_{10}S$) as DMBT], as Au has only one isotope. The minor differences with calculated patterns (fig. S1, C and D) are due to the slight isotopic impurity, as the isotope enrichment was ~98%. Upon mixing an equimolar mixture of $[^{107}Ag_{25}(DMBT)_{18}]^-$ and $[^{109}Ag_{25}(DMBT)_{18}]^-$ in solution at room temperature, the spectrum changed instantaneously, and the resulting distribution is shown in Fig. 1B. No peaks due to the parent clusters were observed, indicating that they were totally exchanged in this process. The mass spectral distribution calculated (fig. S2A) considering a system where each isotope of Ag (107/109) has a probability of occupying 50% of the total sites of the cluster is similar to the distribution observed in Fig. 1B. It is nearly identical to that of the ion $[Ag_{25}(DMBT)_{18}]^-$, having the natural isotope distribution (^{107}Ag: 51.839%, ^{109}Ag: 48.161%), and the minor differences arise as the ^{107}Ag/^{109}Ag ratio is not exactly 1:1 in nature (fig. S2B). The two isotopically pure clusters were further mixed at varying molar ratios, and in each case, rapid exchange between the two clusters resulted in a binomial mass spectral distribution (fig. S3), in agreement with the calculated isotope pattern considering the relative abundance of each isotope from their initial molar ratio of mixing (fig. S4). Such an equilibrium statistical distribution is expected for a system where there are nearly equivalent sites that have equal probability of exchange.

Control over the exchange dynamics was achieved by lowering the temperature. The parent solutions were cooled to −20°C and mixed in a 1:1 molar ratio, and ESI MS was measured instantly. The source and desolvation temperatures were lowered to 30°C, and the sample was infused from an external syringe, which was also cooled to −20°C to reduce the effect of temperature during injection. In Fig. 2 (A to D), we presented the intermediate stages involving stepwise exchange of the isotopes of the atoms between the two clusters. Although the reaction kinetics was slower at lower temperatures, the equilibrium distribution was attained in about 30 s. Rapid exchange occurred even in alloys of the cluster (*14*), such as $[Ag_{24}Au(SR)_{18}]^-$ (fig. S5).

To probe how the dynamics of the exchange process is controlled by the inherent structures of the cluster, we performed a similar study

[1]DST Unit of Nanoscience (DST UNS) and Thematic Unit of Excellence (TUE), Department of Chemistry, Indian Institute of Technology Madras, Chennai 600 036, India. [2]Department of Chemical, Biological and Macromolecular Sciences, S. N. Bose National Centre for Basic Sciences, Sector III, Block JD, Salt Lake, Kolkata 700098, India.
*Corresponding author. Email: pradeep@iitm.ac.in

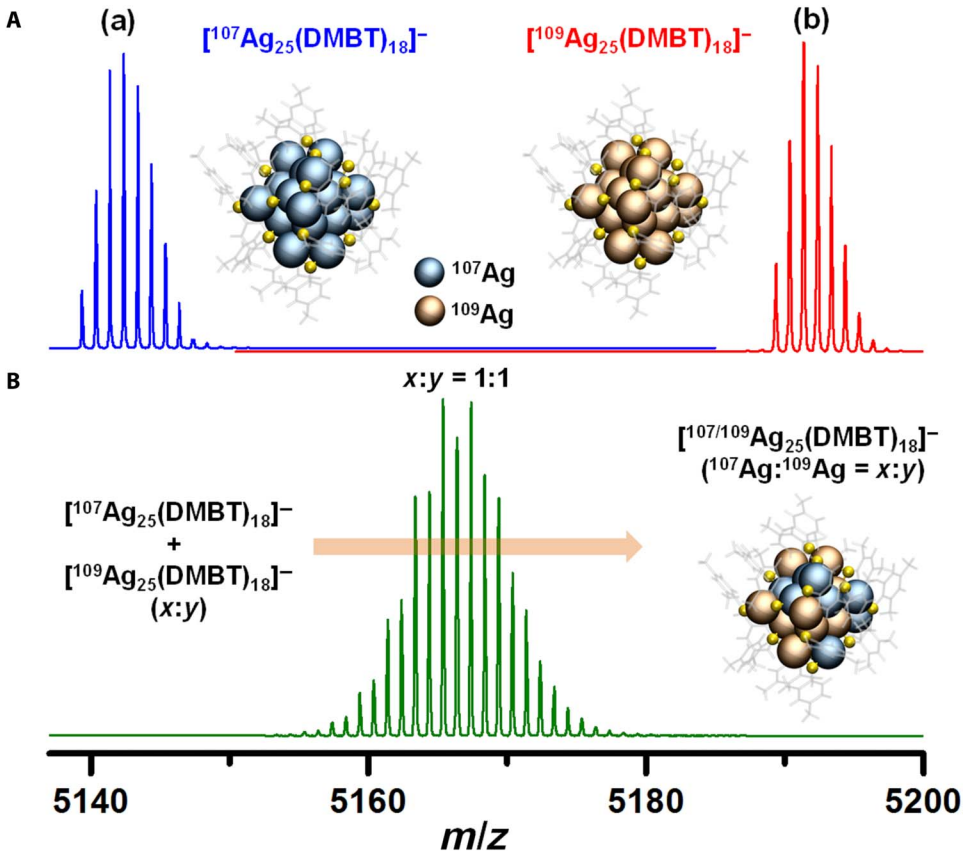

Fig. 1. Mass spectra of the parent isotope clusters and the product of mixing. (**A**) ESI MS of the as-synthesized isotopically pure clusters, (a) $[^{107}Ag_{25}(DMBT)_{18}]^-$ and (b) $[^{109}Ag_{25}(DMBT)_{18}]^-$. (**B**) Mass spectral distribution of the product obtained by mixing the two isotopic clusters at 1:1 molar ratio. The spectrum was collected within 1 min after mixing the solutions of the clusters at room temperature. A representation of the clusters is shown. Comparison with the calculated mass spectrum is presented in figs. S1 and S2. Yellow, S; transparent gray, ligands.

with $[Ag_{29}(BDT)_{12}(TPP)_4]^{3-}$, where the dithiolate protection provides a very different structure (*11*) as compared to that of $[Ag_{25}(DMBT)_{18}]^-$. Isotopically pure $[^{107}Ag_{29}(BDT)_{12}(TPP)_4]^{3-}$ (BDT = benzene dithiol) and $[^{109}Ag_{29}(BDT)_{12}(TPP)_4]^{3-}$ clusters were synthesized and characterized using optical absorption (fig. S6C) and ESI MS (fig. S6, A and B). We observed a reduced exchange rate compared to that of $[Ag_{25}(DMBT)_{18}]^-$. At room temperature, an equimolar mixture of the two isotopic $[Ag_{29}(BDT)_{12}(TPP)_4]^{3-}$ clusters, at a concentration of 1.5×10^{-3} mM, showed stepwise exchanges reaching a dynamic equilibrium over a period of 3 hours (fig. S7A). Although the labile TPP ligands were lost during ionization, the use of soft ionization conditions enabled us to observe that exchange occurred at a similar rate to that in the intact TPP-protected clusters that exist in solution (fig. S7B). The clusters mixed at any arbitrary molar ratios also attained equilibrium in a similar manner, and in all cases, the relative abundance of the isotopes in the final product was in accordance with their initial molar ratio of mixing (fig. S8).

The slower exchange rates seen here encouraged us to analyze the dynamics in greater detail. A kinetic plot of the percentage of unexchanged parent isotopic cluster (C_t) versus time (t) is shown in Fig. 3. At a given time, the percentage of exchange on either of the two isotopic clusters was similar when mixed in equimolar quantities. Therefore, monitoring the kinetics with respect to either of them gave identical results. In this plot, we included a hypothetical data point at $t = 0$ min and $C_t = 100\%$, assuming that at 0 min, that is, in an ideal situation before mixing, the abundance of a particular isotope ($^{107}Ag/^{109}Ag$) in the clusters is 100%. Figure 3 shows that at room temperature (25°C), the $^{107}Ag/^{109}Ag$ exchange rate was initially fast, and within 8 to 10 min, about 30% exchange occurred. Later, the exchange progressed slowly, and after about 250 min, the rate slowed down further, approaching an equilibrium corresponding to a state of 50% exchange. A triexponential effectively fitted the data points, suggesting at least three different rates for the exchange process with rate constants of 5.9×10^{-1} min^{-1}, 1.4×10^{-2} min^{-1}, and 7.1×10^{-18} min^{-1}, respectively. Similar exchange was studied at higher temperatures of 40° and 60°C (fig. S9, A and B), and the kinetic plots are shown in the inset of Fig. 3. The rate increased substantially at higher temperatures, and the reaction was complete within 60 min, whereas upon cooling the reaction mixture to 0°C the rate was drastically reduced and the process took around 3 days to attain equilibrium (fig. S9, C and D). Similar features were also observed for H/D exchange in supramolecular polymers in water (*15*). The three stages of exchange suggest that possibly the isotopic exchange in nanoparticles proceeds through (i) rapid exchange of their surface atoms, (ii) slower diffusion of the exchanged atoms within the core, and (iii) subsequent equilibration in the whole cluster. The reaction rates were dependent on the concentration of the clusters, which was evident from the kinetic studies at lower (1.5×10^{-5} mM) and higher (1.5×10^{-1} mM) concentrations compared to the above case (1.5×10^{-3} mM) (fig. S10). At a given concentration of the parent clusters, we also

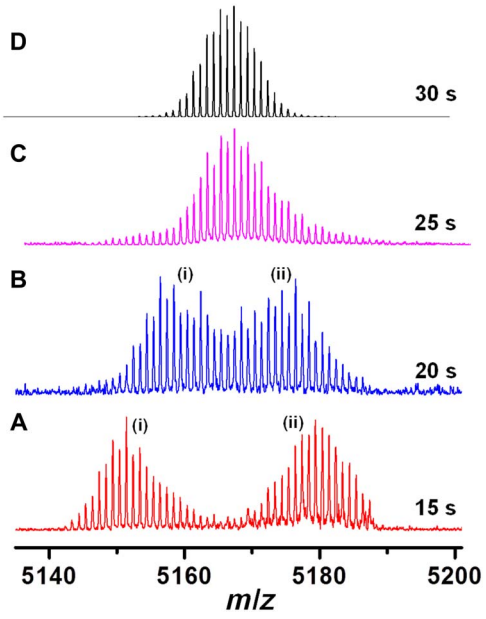

Fig. 2. Low-temperature reaction showing the intermediate steps of exchange. Exchange between the two isotopic $[Ag_{25}(DMBT)_{18}]^-$ clusters at −20°C showing the intermediate stages of exchange (**A**) to (**D**) with mixing time (s). Distributions (i) and (ii) denote exchange at the $[^{107}Ag_{25}(DMBT)_{18}]^-$ and $[^{109}Ag_{25}(DMBT)_{18}]^-$ sides, respectively. Noise in the spectrum is due to the short acquisition time.

investigated the reaction rates at different molar ratios of mixing. Keeping the total number of moles of the mixture as constant, and starting from an excess concentration of $[^{107}Ag_{29}(BDT)_{12}(TPP)_4]^{3-}$, the rate increases with an increase in the concentration of $[^{109}Ag_{29}(BDT)_{12}(TPP)_4]^{3-}$, reaching a maximum at 1:1 condition. As the relative concentration of $[^{109}Ag_{29}(BDT)_{12}(TPP)_4]^{3-}$ in the reaction mixture increases, the number of effective collisions between the isotopically different entities increases, and hence, the rate of exchange increases. Similar results were obtained starting from an excess concentration of $[^{109}Ag_{29}(BDT)_{12}(TPP)_4]^{3-}$ and slowly increasing the concentration of $[^{107}Ag_{29}(BDT)_{12}(TPP)_4]^{3-}$ in the mixture. Kinetic studies at different molar ratios showing the rate constants (fig. S11) and corresponding time-dependent ESI MS (fig. S12) are included in the Supplementary Materials. Reaction rates were independent of solvents such as dimethyl formamide (DMF), acetonitrile (ACN), and dichloromethane (DCM).

To investigate the mechanism and the driving forces of the isotopic exchange reaction, we carried out molecular docking studies and free-energy calculations. The mechanism of atom exchange is expected to be initiated through intercluster collisions (*16*), and this expectation is consistent with the temperature dependence of the rate constants. We have carried out molecular docking simulations for studying the interaction between two $[Ag_{25}(DMBT)_{18}]^-$ and two $[Ag_{29}(BDT)_{12}(TPP)_4]^{3-}$ clusters. In each case, docking generated 10 different possible orientations, and the lowest-energy geometries for the approach of two $[Ag_{25}(DMBT)_{18}]^-$ and two $[Ag_{29}(BDT)_{12}(TPP)_4]^{3-}$ clusters are represented in Fig. 4 (A and B). However, the other possible geometries were also similar in both cases, where the two clusters approach along the same orientation or along other symmetry equivalent orientations such that they interact at similar sites and generate the same configuration. The other possibilities were also energetically similar within 0.01 to 0.07 kcal/mol. As all the possible structures obtained from docking were geometrically and energetically equivalent, it is likely that exchange reaction will be more favorable when the clusters approach along this specific geometry. The FFGMG obtained by docking two $[Ag_{25}(DMBT)_{18}]^-$ clusters indicates that after collision, the clusters may bind together supramolecularly in the initial steps of the reaction with an interaction energy of −23.7 kcal/mol between the two clusters (Fig. 4A). The rapid exchange and the structural changes in $[Ag_{25}(DMBT)_{18}]^-$ can also be viewed from their topologically simplified structure (referred to as the aspicule model) (*17*), which considers the structure of an $M_{25}L_{18}$ cluster (where M = Au, Ag; L = ligand) as a system of three interlocked Borromean rings of $M_8(SR)_6$ around a central M atom. Rapid exchange of isolobal $Ag_2(SR)_3$ and $Ag(SR)_2$ entities may occur. The opening of the rings can also make the core more exposed and facilitate spontaneous exchange of Ag or Ag-SR units between the core and staples of the two clusters. In comparison, $[Ag_{29}(BDT)_{12}(TPP)_4]^{3-}$ does not contain any interlocked rings or chain structures. It has a rigid surface network with cross-linking dithiolates in the outer shell. In the lowest-energy geometry of two $[Ag_{29}(BDT)_{12}(TPP)_4]^{3-}$ clusters (Fig. 4B), the proximity of Ag_3S_6 or AgS_3P motifs of the two clusters may result in opening up of these staples. Molecular docking reveals an interaction energy of −7.8 kcal/mol between two $[Ag_{29}(BDT)_{12}(TPP)_4]^{3-}$ clusters (Fig. 4B). The supramolecular interactions between the clusters mainly include van der Waals and C-H···π interactions. In the case of $[Ag_{25}(DMBT)_{18}]^-$ clusters, the H of the benzene ring and $-CH_3$ group of one ligand on a cluster can interact with the π-system of the benzene ring of another cluster to facilitate the binding. These C-H···π interaction distances are in the range of 2.99 to 4.16 Å, which are comparable with the C-H···π distances observed in the crystal structures of Au_{246} (*18*) and Ag_{29} (*19*) nanoclusters. Interactions are also similar in the case of $[Ag_{29}(BDT)_{12}(TPP)_4]^{3-}$ clusters. The C-H···π interactions exist between –H of BDT of one cluster with benzene ring of BDT of another cluster at a distance of about 3.46 to 4.39 Å. The interactions are greater in the $[Ag_{25}(DMBT)_{18}]^-$ cluster, leading to higher binding energy. The interactions between the ligands are indicated in fig. S13. The reduced intercluster interaction energy and higher rigidity in the structure of $[Ag_{29}(BDT)_{12}(TPP)_4]^{3-}$ might result in a slower exchange rate as compared to that of $[Ag_{25}(DMBT)_{18}]^-$. However, more detailed computations are required to understand the complete mechanism of the atom exchange process.

We considered the thermodynamics of the reaction to identify the main driving force of the isotopic exchange reaction. The energy barrier for an intercluster isotopic exchange represents the energy cost of breaking and reforming bonds and any intermediate barriers, which must be crossed while the atoms travel along the path from their initial to final positions. We computed the enthalpic [electronic energy, zero-point energy (ZPE), and specific heat] and the entropic (electronic, translational, rotational, and vibrational) contributions to the free energy. Computational details are mentioned in Materials and Methods, and detailed results are presented in table S2. The total electronic energies of the clusters do not vary when different isotopes of the atoms are exchanged and rearranged because their bonding interactions are identical. Hence, any differences in enthalpy will be due to ZPE. Furthermore, the vibrational contribution to enthalpy and entropy will also contribute to the free energy. However, we found that there were only very small differences in the free energy of the clusters (~0.01 eV) due to isotopic exchange, and moreover, these differences cancel out when the reaction free energy [$\Delta G_{react} = G(\text{products}) - G(\text{reactants})$] is computed for the 1:1 ratio. In this calculation, we

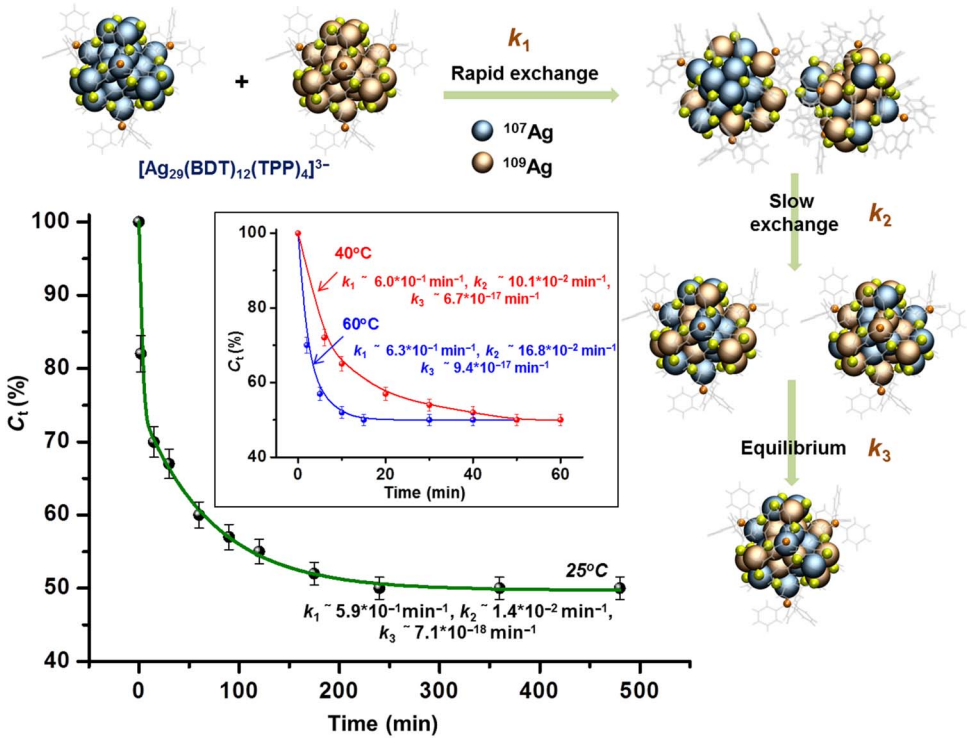

Fig. 3. Kinetic study of isotopic exchange in $[Ag_{29}(BDT)_{12}(TPP)_4]^{3-}$ clusters. Plot of percentage of unexchanged parent isotopic cluster (C_t) versus time (min) of reaction at room temperature (25°C). Kinetics at 40° and 60°C are presented in the inset. Average of three kinetic measurements is plotted, and the error bar is indicated at each point. A schematic showing the different stages of isotopic exchange is also shown in the figure. Yellow, S; orange, P; transparent gray, ligands.

have assumed that the parent clusters are the isotopically pure reactants and that the products are the two mixed isotope clusters with the following compositions: (*m*,*n*) = (12,13) and (13,12) in the case of $[^{107}Ag_m{}^{109}Ag_n(DMBT)_{18}]^-$ and (*m*,*n*) = (14,15) and (15,14) in the case of $[^{107}Ag_m{}^{109}Ag_n(BDT)_{12}(TPP)_4]^{3-}$. Thus, in the absence of other contributions to the reaction free energy, the contribution from the mixing of isotopic clusters is expected to be of central importance in understanding the driving force of the reaction.

We now describe how we estimated the mixing contribution to the free energy. Application of the concept of entropy to a single cluster is not proper due to the small number of atoms (10^2 to 10^3) in an individual cluster; however, we may apply it to the macroscopically large ensemble of *N* clusters, and the ensemble configuration is defined by the positions of ^{107}Ag and ^{109}Ag atoms in *N* clusters, where *N* is taken to be in the thermodynamic limit. The final equilibrium state of the cluster ensemble will be that in which the number of isotopic substituents is maximum for a given molar ratio so that the whole ensemble of clusters has the highest entropy (S), which is defined as S = *k*log*W*, where *W* is the total number of ways of arranging the two isotopes of Ag atoms (microstates) in the total available sites of the clusters, and *k* is the Boltzmann constant. For the equimolar composition, this will occur for the half-mixed compositions of each clusters, that is, *n* = (12, 13) and (13, 12) for Ag_{25}, and (14, 15) and (15, 14) for Ag_{29}, where these compositions have the identical maximum degeneracy in positional arrangements.

We approximate the ensemble of clusters with two crystalline lattices, one consisting of ^{107}Ag and the other of ^{109}Ag, which are fused together, and then assume random thermal exchanges of atoms in the joint lattice. In this simplification, we considered only the Ag atoms, neglecting the cluster structure and symmetry and all interatomic interactions, and this situation is identical to the mixing of two ideal gases. Hence, the expression for mixing or configurational entropy is simply that of mixing two different ideal gases, which is known from statistical mechanics, and is given by

$$\Delta S_{mix} = -n_{mol}R[p\ln p + (1-p)\ln(1-p)]$$

where *p* is the mole fraction of ^{107}Ag, (1 − *p*) is the mole fraction of ^{109}Ag, and n_{mol} is the total number of moles of the mixture. ΔS_{mix} attains its maximum negative value for the half-and-half mixture, that is, *p* = 0.5, for a given total number of moles of the mixture (*20*). For a 1:1 ratio of mixing, ΔS_{mix} is *R*ln2 = 5.76 J K^{-1} mol^{-1}, which is 1.37 cal K^{-1} mol^{-1}, and $\Delta G_{mix} = -T^*\Delta S_{mix} = -408.26$ cal mol^{-1} (*T* = 298 K and n_{mol} = 1). Because the calculated reaction free energies are negligible, the mixing entropic contribution to the free energy must be the main driving force of the observed spontaneous reaction. We remark that the mixing entropy term would also be important in spontaneous bimetallic intercluster reactions, where there are larger enthalpic changes due to the bonding interactions such as those between $Ag_{25}(DMBT)_{18}$ and $Au_{25}(PET)_{18}$ (*16*).

DISCUSSION

The results presented establish that spontaneous isotopic exchange can occur between atomically precise silver nanoclusters. While it is rapid in $[Ag_{25}(SR)_{18}]^-$, it is relatively slower in $[Ag_{29}(S_2R)_{12}(TPP)_4]^{3-}$, reflecting the differences in their chemical structures. Spontaneity in such reactions, driven by their entropy of mixing, reflects the dynamic

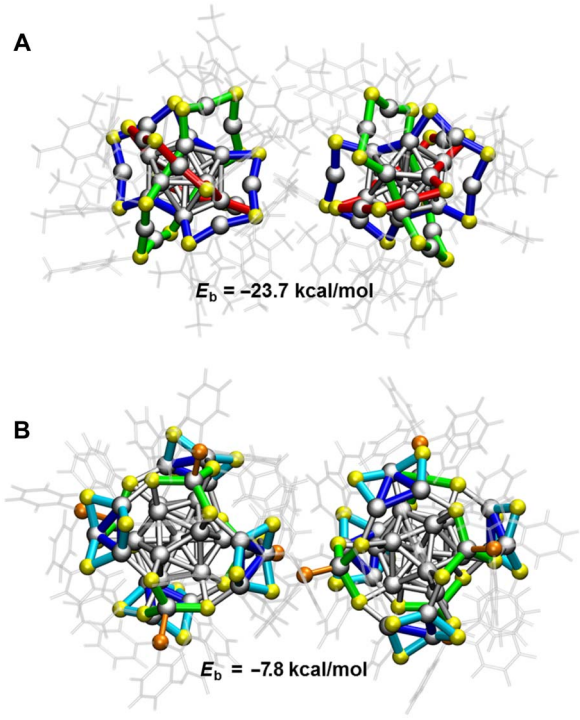

Fig. 4. Molecular docking studies. Force-field global minimum geometry (FFGMG) of two (**A**) $[Ag_{25}(DMBT)_{18}]^-$ and (**B**) $[Ag_{29}(BDT)_{12}(TPP)_4]^{3-}$ clusters, lying in close proximity. Gray, Ag; yellow, S; orange, P. The overlapping Borromean rings are shown in blue, green, and red in (A); staple units are shown in green and blue in (B); and ligand shell is shown in transparent gray. Atomic diameters were reduced to show the bonding.

nature of nanoparticles in solution. However, our study is restricted only to subnanometer-sized clusters, where exchange is shown to be dependent on their inherent structures. In a similar manner, the study may also be extended to classic nanomaterials of various sizes. Future possibilities include investigating the correlation between the extent of exchange with the size of the nanoparticles and the nature of their ligands or the constituent metal atoms.

The fundamental significance of this study is to understand the dynamics in nanoscale systems, which is comparable to solution-state dynamics of many simpler molecules like H_2O. This study has the potential to answer questions regarding the rigidity of the structures and rapid interconversions between the subunits that constitute nanosystems. Nanoparticle dynamics contributing to catalysis is of relevance to applications. In homogeneous catalysis involving nanoparticles, the site at which chemistry occurs could be changing continuously. This characteristic implies associated dynamics for the anchored ligands and therefore may contribute to their solution-state availability. This phenomenon may also be important in biology, where nanoparticles are used as carriers of molecular cargo.

Moreover, isotopic exchanges like H/D exchanges in H_2O/D_2O (*21*) can alter physical and chemical properties of the materials. Isotopic exchange affects the vibrational modes. In the case of clusters also, there will be changes in the vibrations, although these were found to be very small from our calculations. The change in properties is small in this particular case probably because the mass ratio of the two isotopes of Ag (109/107) is 1.019 (in contrast, the mass ratio for other isotopes like D/H is ~2), and hence, the effect will be less compared to the total mass of the cluster. However, the effect of isotopic exchange may become significant to alter the properties with the appropriately chosen cluster system and appropriately chosen metal or ligand isotopes. Isotopic modification can introduce a change in both the spatial distribution of nuclear mass and the nuclear spins in the clusters. Because the x-ray diffraction pattern of mixed isotope clusters and single isotope clusters would be identical, the use of neutron scattering could be useful to probe the structure and dynamics of these clusters. The change in the nuclear spins would affect the nuclear magnetic resonance (NMR) spectrum, and in the case of clusters with an unpaired electronic spin, isotopic modification would change the electron spin resonance properties through the electron-nuclear hyperfine interactions, which depend on the values of the nuclear spins. For example, in the case of isotopes of metals such as Pd (^{102}Pd, ^{104}Pd, ^{105}Pd, ^{106}Pd, ^{108}Pd, and ^{110}Pd), ^{105}Pd has a nuclear spin of (5/2)+, while other isotopes have 0 nuclear spin. This is similar in the case for the isotopes of Pt (^{192}Pt, ^{194}Pt, ^{195}Pt, ^{196}Pt, ^{198}Pt), where ^{195}Pt has a nuclear spin of (1/2)–, while other isotopes have 0 nuclear spin. Such isotopic modification in clusters and their crystals might have applications in magnetic devices.

MATERIALS AND METHODS

Reagents and materials

Isotopically pure Ag foils, ^{107}Ag (98%) and ^{109}Ag (98%), were purchased from Cambridge Isotope Laboratories Inc. 2,4-DMBT, 1,3-BDT, sodium borohydride ($NaBH_4$), and tetraphenyl phosphonium bromide (PPh_4Br) were purchased from Sigma-Aldrich. Triphenyl phosphine (TPP) was purchased from Spectrochem, India. All the solvents [DCM, methanol (MeOH), DMF, and ACN] were of the high-performance liquid chromatography grade and were used without further purification.

Synthesis of isotopically pure silver nitrate ($^{107}AgNO_3$ and $^{109}AgNO_3$) from isotopically pure metal foils (^{107}Ag and ^{109}Ag)

About 50 mg of the metal foils of the isotopes of Ag (^{107}Ag and ^{109}Ag) was separately reacted with about 2 ml of concentrated nitric acid (70%) in a 5-ml reaction vessel and heated at 70°C inside a fume hood. The heating was continued until the evolution of nitrogen oxide gases was complete and the solution turned colorless. The solution was then diluted with water, and heating was continued. The process of addition of water was continued for a few times, and lastly, 0.5 ml of a concentrated solution of $AgNO_3$ was kept for crystallization. For crystallization, the solution was kept inside an airtight dark box in the presence of solid P_2O_5 and NaOH pellets (kept separately in the same box) to enhance the evaporation of water and remove excess acid. Colorless crystals of $AgNO_3$ were obtained within 5 to 7 days. The yield of the reaction was around 95%.

Synthesis of isotopically pure $[^{107}Ag_{25}(DMBT)_{18}]^-[PPh_4]^+$ and $[^{109}Ag_{25}(DMBT)_{18}]^-[PPh_4]^+$ clusters

Isotopically pure clusters were synthesized using the isotopically pure $AgNO_3$ salt, which was synthesized according to the above mentioned method. The clusters were synthesized following a reported protocol (*9*). About 38 mg of $^{107}AgNO_3/^{109}AgNO_3$ was dissolved in a mixture of 2 ml of methanol and 17 ml of DCM. To this reaction mixture, about 90 μl of 2,4-DMBT was added. The mixture was kept under stirring condition at 0°C. About 6 mg of PPh_4Br in 0.5 ml of methanol was added after about 15 to 20 min. Next, about 15 mg of $NaBH_4$ in 0.5 ml of ice-cold water was added to the solution in a dropwise fashion. The stirring was continued for about 7 to 8 hours; the solution was then stored at 4°C for about 2 days. For purification, the sample

was centrifuged and DCM was removed by rotary evaporation. The precipitate was washed twice with methanol. Then, the cluster was redissolved in DCM and centrifuged to remove any further insoluble impurities. Further removal of DCM by rotary evaporation led to the formation of the purified clusters ($[^{107}Ag_{25}(DMBT)_{18}]^-[PPh_4]^+$/$[^{109}Ag_{25}(DMBT)_{18}]^-[PPh_4]^+$) in their powder form.

Synthesis of isotopically pure $[^{107}Ag_{29}(BDT)_{12}(TPP)_4]^{3-}$ and $[^{109}Ag_{29}(BDT)_{12}(TPP)_4]^{3-}$ clusters

Isotopically pure clusters were synthesized using the isotopically pure $AgNO_3$ salt following a reported method (*10*). About 20 mg of $^{107}AgNO_3$/$^{109}AgNO_3$ was dissolved in a mixture of 5 ml of MeOH and 10 ml of DCM. To this solution, about 13.5 μl of 1,3-BDT ligand was added, and the reaction mixture was kept under stirring condition. Addition of the thiol immediately resulted in a turbid yellow solution, which turned clear upon addition of about 200 mg of PPh_3. After about 15 min, a freshly prepared solution of 10.5 mg of $NaBH_4$ in 500 μl of water was added. The stirring was continued under dark conditions for 3 to 5 hours. During the course of the reaction, the dark brown color of the solution changed to orange. After completion of the reaction, the mixture was centrifuged and the supernatant was discarded. The precipitate consisting of the Ag_{29} cluster was washed repeatedly with methanol. The sample was dissolved in DMF and again centrifuged to remove any further insoluble contaminants. The supernatant was vacuum dried, and the purified clusters ($[^{107}Ag_{29}(BDT)_{12}(TPP)_4]^{3-}$/$[^{109}Ag_{29}(BDT)_{12}(TPP)_4]^{3-}$) were obtained in powder form.

Synthesis of isotopically pure $[^{107}Ag_{24}Au(DMBT)_{18}]^-$ and $[^{109}Ag_{24}Au(DMBT)_{18}]^-$ clusters

Isotopically pure $[^{107}Ag_{25}(DMBT)_{18}]^-$ and $[^{109}Ag_{25}(DMBT)_{18}]^-$ clusters were used as the precursor to which Au^+ was added in a controlled manner such that galvanic replacement of a Ag atom with Au resulted in the formation of $[^{107}Ag_{24}Au(DMBT)_{18}]^-$ and $[^{109}Ag_{24}Au(DMBT)_{18}]^-$ clusters (*13*), respectively.

Reaction of the isotopically pure clusters

In each case, stock solutions of parent isotopically pure clusters were prepared at a concentration of 1.5×10^{-3} mM. Then, they were mixed in different molar ratios, and their reaction was monitored by ESI MS.

Instrumentation

The optical absorption spectra were measured in PerkinElmer Lambda 25 ultraviolet-visible spectrophotometer. All the mass spectrometric measurements were done in a Waters SYNAPT G2-Si instrument. The instrument is well equipped with ESI, and all spectra were measured in the negative ion and resolution mode. The instrument is capable of measuring ESI MS with high-resolution touching orders of 50,000 ($m/\Delta m$). The instrument was calibrated using NaI. An optimized condition involving a capillary voltage of 3 kV, a cone voltage of 20 V, a desolvation gas flow of 400 liters/hour, a source temperature of 100°C, a desolvation temperature of 150°C, and a sample infusion rate of 30 μl/hour was used for all measurements. For low-temperature measurements, the source and desolvation temperatures were lowered to 30°C, and the sample was infused by an external syringe, which was also cooled at −20°C.

Computational methods

Free-energy calculations

The exchange effect of silver isotopes (^{107}Ag and ^{109}Ag) was computationally studied in $[Ag_{25}(DMBT)_{18}]^-$ and $[Ag_{29}(BDT)_{12}(PPh_3)_4]^{3-}$ clusters by calculating free energy and thermochemistry parameters such as ZPE, enthalpy (H), and entropy (S) using density functional theory (DFT), as implemented in real-space grid-based projector augmented wave (PAW) package (*22*). The PAW setup $Ag(4d^{10}5s^1)$, $S(3s^23p^4)$, $P(3s^23p^3)$, $C(2s^22p^2)$, and $H(1s^1)$ was considered to include only the valence electronic structure for the constituent atoms including the scalar-relativistic effects for Ag. Further, a reduced model was used considering $-CH_3$ instead of the benzene rings in DMBT, BDT, and TPP ligands to reduce the high computational time of frequency calculations. The real-space calculation in finite difference mode, along with Perdew-Burke-Ernzerhof (PBE) functional, was applied for the geometry optimizations with a grid spacing of 0.2 Å, and the minimization criterion was the residual forces of 0.05 eV/Å, without considering any symmetry constraints. The atomic masses of Ag isotopes were taken as 106.905 and 108.905 for ^{107}Ag and ^{109}Ag, respectively. The vibrational modes were calculated only for Ag, S, and P atoms using the finite difference approximation of the Hessian matrix by considering the two displacements ($+\Delta$ and $-\Delta$) per atom in each Cartesian coordinate. Further, the calculated vibrational energies were used to calculate the thermodynamic quantities like *H*, *S*, and Gibbs free energy (*G*).

The calculation of *G* is made in the ideal gas approximation. It includes the electronic energy (E_{pot}), ZPE (E_{ZPE}), translational, rotational, and vibrational components of H and S, which are based on DFT calculations. An additional entropy of mixing component was calculated separately from statistical mechanics.

Enthalpy (*H*) is calculated within the atomistic simulation environment as

$H = E_{pot} + E_{ZPE} + C_{v\_trans} + C_{v\_rot} + C_{v\_vib}$, and entropy is $S = S_{trans} + S_{rot} + S_{elec} + S_{vib}$

Hence, the Gibb's free energy at temperature *T* and pressure *P* is calculated as

$$G = H - T^*S$$

The structural isomers of each isotopically substituted cluster arising from the different possible ways of arranging *n* Ag isotopic substituent atoms among the total number of Ag atoms are all degenerate as far as their total electronic energy is concerned, with a small difference of only 0.01 eV for both Ag_{29} and Ag_{25} in the value of G of the parent and isotopic substituent clusters, in terms of their enthalpic and the vibrational entropic components (see table S2).

We may write the reaction equations for the 1:1 ratio of mixing as follows, and in doing so, we assume that both products, (*m*,*n*) = (12,13) and (13,12) for Ag_{25} and (*m*,*n*) = (14,15) and (15,14) for Ag_{29}, are equally likely to form.

$$[^{107}Ag_{25}(DMBT)_{18}]^- + [^{109}Ag_{25}(DMBT)_{18}]^- \rightarrow [^{107}Ag_{13}{}^{109}Ag_{12}(DMBT)_{18}]^- + [^{107}Ag_{12}{}^{109}Ag_{13}(DMBT)_{18}]^-$$

For the case of $[Ag_{29}(BDT)_{12}(TPP)_4]^{3-}$

$$[^{107}Ag_{29}(BDT)_{12}(TPP)_4]^{3-} + [^{109}Ag_{29}(BDT)_{12}(TPP)_4]^{3-} \rightarrow [^{107}Ag_{15}{}^{109}Ag_{14}(BDT)_{12}(TPP)_4]^{3-} + [^{107}Ag_{14}{}^{109}Ag_{15}(BDT)_{12}(TPP)_4]^{3-}$$

For (*m*,*n*) = (12,13), (13,12) in $[Ag_{25}(DMBT)_{18}]^-$ and (*m*,*n*) = (14,15), (15,14) in $[Ag_{29}(BDT)_{12}(TPP)_4]^{3-}$ substituent cases (1:1 molar ratio), we have computed the reaction molar Gibbs free energy (ΔG_{react}) at standard temperature (298 K) and pressure (1 atm). The reaction free

energies (ΔG_{react}) are zero for both Ag_{29} and Ag_{25} clusters (see table S2), and the overall free energy of reaction is given by

$$\Delta G = \Delta G_{react} + \Delta G_{mix} = G(\text{products}) - G(\text{reactants}) + \Delta G_{mix}$$

For $[Ag_{25}(DMBT)_{18}]^-$,

$$G(\text{products}) = G \text{ of } {}^{107}Ag^{109}Ag(12,13) + G \text{ of } {}^{107}Ag^{109}Ag(13,12)$$
$$G(\text{reactants}) = G \text{ of parent } {}^{107}Ag_{25} + G \text{ of parent } {}^{109}Ag_{25}$$

and similarly for Ag_{29}.

The expression for mixing or configurational entropy is simply that of mixing two different ideal gases, which is known from statistical mechanics, and is given by

$$\Delta S_{mix} = -n_{mol}R[(p\ln p + (1-p)\ln(1-p)]$$

where p is the mole fraction of ^{107}Ag, $(1 - p)$ is the mole fraction of ^{109}Ag, and n_{mol} is the total number of moles of the mixture (*17*). We note that the mixing entropy is independent of the cluster size and only depends on the mixing ratio; hence, we expect the half-and-half-mixture to have the largest mixing free energy. For the 1:1 mixture, we have $p = 0.5$, and hence, ΔS_{mix} is $R\ln 2$ ($n_{mol} = 1$) and $\Delta G_{mix} = -T^*\Delta S_{mix} = -RT\ln 2$, where R is the gas constant in joules per mole and $n_{mol} = 1$. This analysis reveals that the entropy of isotopic mixing is the largest and most significant contribution to the Gibbs free energy. Because of the fractional mixing ratio, the mixing entropy is always positive, and therefore, ΔG_{mix} is always negative and is larger than the other terms in the free energy. Hence, ΔG_{mix}, being the largest contribution to the overall reaction, causes ΔG to be always negative, which makes the reaction spontaneous.

The mixing ratio $x = 0.5$ corresponds to the nearest integer numbers of exchanged Ag atoms to half of the total number of Ag atoms in the cluster, because both clusters have an odd number of Ag atoms, for example, (25/2) = 12.5, hence, (13,12) or (12,13), where these compositions both have the identical maximum degeneracy in arrangements as a function of the number of substituents n in the Ag_{25} cluster. Similarly, for the Ag_{29} cluster, (29/2) = 14.5 and, hence, (14,15) or (15,14) are the most entropically favorable compositions in Ag_{29}.

Molecular docking

To understand the intermolecular interactions in $[Ag_{25}(SR)_{18}]^-$ clusters, molecular docking studies were performed using AutoDock4.2 and its associated tools (*23*). DFT-optimized geometry and partial charges of $[Ag_{25}(SR)_{18}]^-$ were used for this study. We used $[Ag_{25}(SR)_{18}]^-$ as both "ligand" and "receptor." Receptor grids were generated using 126 × 126 × 126 grid points in *xyz*, with a grid spacing of 0.375 Å, and map types were created using AutoGrid-4.2. The grid parameter file (.gpf) was saved using MGL Tools-1.4.6.50. The docking parameter files (.dpf) were generated using MGLTools-1.4.6.50. The results of AutoDock generated an output file (.dlg), and the generated conformers were scored and ranked as per the interaction energy. Ten lowest-energy conformers were obtained. We used the Lamarckian genetic algorithm for the output file using MGLTools-1.4.6. The binding free energy of the FFGMG of the dimeric cluster adduct was −23.7 kcal/mol. Similar study was done with $[Ag_{29}(S_2R)_{12}(TPP)_4]^{3-}$ clusters, where $[Ag_{29}(S_2R)_{12}(TPP)_4]^{3-}$ was used as both ligand and receptor. In this case, the binding free energy of FFGMG of the dimeric adduct was −7.8 kcal/mol.

Calculation of theoretical isotope patterns with varying composition of $^{107}Ag/^{109}Ag$

We calculated the theoretical isotope patterns of $[Ag_{25}(DMBT)_{18}]^-$ and $[Ag_{29}(BDT)_{12}(TPP)_4]^{3-}$ by varying the abundance of each isotope ($^{107}Ag/^{109}Ag$) in them by 1% change so that the composition is (*x*,*y*), that is, {(100,0), (99,1), (98,2).....(0,100)}, where x and y are the abundance of ^{107}Ag and ^{109}Ag, respectively. The experimental spectra were compared with the calculated spectra to find the best match and hence confirm the composition.

Details of fitting the kinetic data

The triexponential fitting in Fig. 3 was performed using the Origin 8.5 software package. The equation $y = k_1\exp(-t^*a) + k_2\exp(-t^*b) + k_3\exp(-t^*c)$ was used for the triexponential fits. The parameters k_1, k_2, k_3, a, b, and c were varied during the fitting, and t was used as the independent variable. Both monoexponential and biexponential fits were inadequate, and only a triexponential fit could successfully fit the data points.

SUPPLEMENTARY MATERIALS

Supplementary material for this article is available at http://advances.sciencemag.org/cgi/content/full/5/1/eaau7555/DC1

Fig. S1. Characterization of isotopically pure $[^{107}Ag_{25}(DMBT)_{18}]^-$ and $[^{109}Ag_{25}(DMBT)_{18}]^-$ clusters.

Fig. S2. Isotope patterns of the product obtained by reaction of $[^{107}Ag_{25}(DMBT)_{18}]^-$ and $[^{109}Ag_{25}(DMBT)_{18}]^-$ at 1:1 molar ratio.

Fig. S3. ESI MS of reaction product obtained by mixing the two isotopic $[^{107}Ag_{25}(DMBT)_{18}]^-$ and $[^{109}Ag_{25}(DMBT)_{18}]^-$ clusters at various molar ratios.

Fig. S4. Comparison of the experimental and calculated isotope patterns of the products obtained by mixing $[^{107}Ag_{25}(DMBT)_{18}]^-$ and $[^{109}Ag_{25}(DMBT)_{18}]^-$ at various molar ratios.

Fig. S5. Isotope exchange in $[Ag_{24}Au(DMBT)_{18}]^-$ clusters.

Fig. S6. Characterization of isotopically pure $[^{107}Ag_{29}(BDT)_{12}(TPP)_4]^{3-}$ and $[^{109}Ag_{29}(BDT)_{12}(TPP)_4]^{3-}$ clusters.

Fig. S7. Reaction between $[^{107}Ag_{29}(BDT)_{12}(TPP)_4]^{3-}$ and $[^{109}Ag_{29}(BDT)_{12}(TPP)_4]^{3-}$ clusters in 1:1 molar ratio at room temperature.

Fig. S8. ESI MS of reaction product obtained by mixing the two isotopic $[^{107}Ag_{29}(BDT)_{12}(TPP)_4]^{3-}$ and $[^{109}Ag_{29}(BDT)_{12}(TPP)_4]^{3-}$ clusters at various molar ratios.

Fig. S9. Time-dependent study of reaction between $[^{107}Ag_{29}(BDT)_{12}(TPP)_4]^{3-}$ and $[^{109}Ag_{29}(BDT)_{12}(TPP)_4]^{3-}$ in 1:1 molar ratio at various temperatures.

Fig. S10. Kinetic study of isotopic exchange at different concentrations of $[Ag_{29}(BDT)_{12}(TPP)_4]^{3-}$ clusters.

Fig. S11. Kinetic study of isotopic exchange in $[Ag_{29}(BDT)_{12}(TPP)_4]^{3-}$ clusters at different molar ratios of mixing.

Fig. S12. Time-dependent study of reaction between $[^{107}Ag_{29}(BDT)_{12}(TPP)_4]^{3-}$ and $[^{109}Ag_{29}(BDT)_{12}(TPP)_4]^{3-}$ at various molar ratios.

Fig. S13. Molecular docking studies.

Table S1. Abundance of ^{107}Ag in product = $\{x/(x + y)\} \times 100$ and ^{109}Ag in product = $\{y/(x + y)\} \times 100$.

Table S2. Table showing ZPE and Gibbs free energy (*G*) values of the isotopic clusters.

REFERENCES AND NOTES

1. H. C. Urey, F. G. Brickwedde, G. M. Murphy, A hydrogen isotope of mass 2. *Phys. Rev.* **39**, 164–165 (1932).
2. G. N. Lewis, R. T. Macdonald, Concentration of H^2 isotope. *J. Chem. Phys.* **1**, 341–344 (1933).
3. A. Thibblin, P. Ahlberg, Reaction branching and extreme kinetic isotope effects in the study of reaction mechanisms. *Chem. Soc. Rev.* **18**, 209–224 (1989).
4. J. W. Pyper, R. S. Newbury, G. W. Barton Jr., Study of the isotopic disproportionation reaction between light and heavy water using a pulsed-molecular-beam mass spectrometer. *J. Chem. Phys.* **46**, 2253–2257 (1967).
5. S.-C. Park, K.-H. Jung, H. Kang, H/D isotopic exchange between water molecules at ice surfaces. *J. Chem. Phys.* **121**, 2765–2774 (2004).
6. L. Konermann, J. Pan, Y.-H. Liu, Hydrogen exchange mass spectrometry for studying protein structure and dynamics. *Chem. Soc. Rev.* **40**, 1224–1234 (2011).
7. G. Pratt, D. Rogers, Homogeneous isotope exchange reactions. H_2/D_2. *J. Chem. Soc. Faraday Trans. 1* **72**, 1589–1600 (1976).

8. I. Chakraborty, T. Pradeep, Atomically precise clusters of noble metals: Emerging link between atoms and nanoparticles. *Chem. Rev.* **117**, 8208–8271 (2017).
9. R. Jin, C. Zeng, M. Zhou, Y. Chen, Atomically precise colloidal metal nanoclusters and nanoparticles: Fundamentals and opportunities. *Chem. Rev.* **116**, 10346–10413 (2016).
10. C. P. Joshi, M. S. Bootharaju, M. J. Alhilaly, O. M. Bakr, $[Ag_{25}(SR)_{18}]^-$: The "Golden" silver nanoparticle. *J. Am. Chem. Soc.* **137**, 11578–11581 (2015).
11. L. G. AbdulHalim, M. S. Bootharaju, Q. Tang, S. Del Gobbo, R. G. AbdulHalim, M. Eddaoudi, D.-E. Jiang, O. M. Bakr, $Ag_{29}(BDT)_{12}(TPP)_4$: A tetravalent nanocluster. *J. Am. Chem. Soc.* **137**, 11970–11975 (2015).
12. M. Zhu, C. M. Aikens, F. J. Hollander, G. C. Schatz, R. Jin, Correlating the crystal structure of a thiol-protected Au_{25} cluster and optical properties. *J. Am. Chem. Soc.* **130**, 5883–5885 (2008).
13. M. W. Heaven, A. Dass, P. S. White, K. M. Holt, R. W. Murray, Crystal structure of the gold nanoparticle $[N(C_8H_{17})_4][Au_{25}(SCH_2CH_2Ph)_{18}]$. *J. Am. Chem. Soc.* **130**, 3754–3755 (2008).
14. M. S. Bootharaju, C. P. Joshi, M. R. Parida, O. F. Mohammed, O. M. Bakr, Templated atom-precise galvanic synthesis and structure elucidation of a $[Ag_{24}Au(SR)_{18}]^-$ nanocluster. *Angew. Chem. Int. Ed.* **55**, 922–926 (2016).
15. X. Lou, R. P. M. Lafleur, C. M. A. Leenders, S. M. C. Schoenmakers, N. M. Matsumoto, M. B. Baker, J. L. J. van Dongen, A. R. A. Palmans, E. W. Meijer, Dynamic diversity of synthetic supramolecular polymers in water as revealed by hydrogen/deuterium exchange. *Nat. Commun.* **8**, 15420 (2017).
16. K. R. Krishnadas, A. Baksi, A. Ghosh, G. Natarajan, T. Pradeep, Structure-conserving spontaneous transformations between nanoparticles. *Nat. Commun.* **7**, 13447 (2016).
17. G. Natarajan, A. Mathew, Y. Negishi, R. L. Whetten, T. Pradeep, A unified framework for understanding the structure and modifications of atomically precise monolayer protected gold clusters. *J. Phys. Chem. C* **119**, 27768–27785 (2015).
18. C. Zeng, Y. Chen, K. Kirschbaum, K. J. Lambright, R. Jin, Emergence of hierarchical structural complexities in nanoparticles and their assembly. *Science* **354**, 1580–1584 (2016).
19. A. Nag, P. Chakraborty, M. Bodiuzzaman, T. Ahuja, S. Antharjanam, T. Pradeep, Polymorphism of $Ag_{29}(BDT)_{12}(TPP)_4^{3-}$ cluster: Interactions of secondary ligands and their effect on solid state luminescence. *Nanoscale* **10**, 9851–9855 (2018).
20. P. Atkins, J. De Paula, *Atkins' Physical Chemistry* (Oxford Univ. Press, 2006).
21. J. D. Bernal, G. Tamm, Zero point energy and physical properties of H_2O and D_2O. *Nature* **135**, 229–230 (1935).
22. J. J. Mortensen, L. B. Hansen, K. W. Jacobsen, Real-space grid implementation of the projector augmented wave method. *Phys. Rev. B* **71**, 035109 (2005).
23. G. M. Morris, R. Huey, W. Lindstrom, M. F. Sanner, R. K. Belew, D. S. Goodsell, A. J. Olson, AutoDock4 and AutoDockTools4: Automated docking with selective receptor flexibility. *J. Comput. Chem.* **30**, 2785–2791 (2009).

Acknowledgments: P.C. thanks the Council of Scientific and Industrial Research (CSIR) for a research fellowship. A.N. thanks IIT Madras for an Institute Doctoral fellowship. G.P. thanks IIT Madras for an Institute Postdoctoral fellowship. We thank the Department of Science and Technology (DST), Government of India for continuous support of our research program. We thank D. Frenkel, University of Cambridge, UK, for useful discussions on the computational part of the work. **Funding:** This work was supported by the Council of Scientific and Industrial Research (CSIR), Indian Institute of Technology Madras and Department of Science and Technology (DST), Government of India. **Author contributions:** P.C. carried out the synthesis and designed and conducted the experiments. P.C. and A.N. carried out the ESI MS measurements. A.N. carried out the molecular docking studies. G.N. and G.P. carried out the DFT calculations. N.B. participated in the experiments. M.K.P. calculated the theoretical mass spectral distributions. G.N. and J.C. supervised the computational part. T.P. proposed the project and supervised the progress. The manuscript was written through contributions of all the authors. **Competing interests:** P.C., A.N., G.N., G.P., and T.P. are inventors of an Indian patent application related to this work (no. 201741037349, filed on 23 October 2017). The other authors declare that they have no competing interests. **Data and materials availability:** All data needed to evaluate the conclusions in the paper are present in the paper and/or the Supplementary Materials. Additional data related to this paper may be requested from the authors.

Submitted 12 July 2018
Accepted 27 November 2018
Published 2 January 2019
10.1126/sciadv.aau7555

Citation: P. Chakraborty, A. Nag, G. Natarajan, N. Bandyopadhyay, G. Paramasivam, M. K. Panwar, J. Chakrabarti, T. Pradeep, Rapid isotopic exchange in nanoparticles. *Sci. Adv.* **5**, eaau7555 (2019).

ScienceAdvances

Rapid isotopic exchange in nanoparticles

Papri Chakraborty, Abhijit Nag, Ganapati Natarajan, Nayanika Bandyopadhyay, Ganesan Paramasivam, Manoj Kumar Panwar, Jaydeb Chakrabarti and Thalappil Pradeep

Sci Adv **5** (1), eaau7555.
DOI: 10.1126/sciadv.aau7555